Sn-Ag-Cu alloy. The Sn-Ag-Cu-Ge alloy solder ball had higher ball shear strength than the Sn-Ag-Cu alloy after an aging test at 150 °C. The Sn-Ag-Cu-Ge alloy solder has better characteristics for both thermal oxidation and thermal reliability test. Therefore, it can be concluded that the Sn-Ag-Cu-Ge alloy is a good candidate to solve the oxidation problem, which is the most critical problem of the Pb-free solder.

Experimental

Two solder ball compositions (in wt%) chosen in this study were : Sn3.0Ag0.5Cu and Sn3.0Ag0.5Cu0.05Ge, and had a diameter of 0.450 mm. The substrate used was CSP with 144 pad openings and each pad was 0.38 mm in diameter. The pads had an electroplated Ni/Au surface finish over Cu trace, with about 0.5 and 5.0 μm in thickness respectively. The solder balls from each composition were bonded to the CSP substrate using a water soluble flux under a reflow oven. The reflow condition is that preheating was done for 2 min at 150 °C, the peak temperature was 235 °C, and the dwell time was 60 sec.

The solder balls after one were then analyzed or subjected to either multiple reflow up to 5 times or aging at 150 °C for a duration up to 500 hs. XPS was utilized to check the oxide layer thickness and examine the surface chemical composition. We assumed that the oxide thickness can be defined by oxygen concentration under three atomic percent. The mechanical joint strength of the bonded balls was evaluated with Dage shear tester using a shear speed of 200 μm/s at a shear height of 10 μm.

Received: August 29, 2005
Final version: September 13, 2005

[1] W. Zhang, C. Liu, D. Li, M. Sui, *Adv. Eng. Mater.* **2004**, *6*, 232.
[2] K. N. Tu, A. M. Gusak, M. Li, *J. Appl. Phys.* **2003**, *93*, 1335.
[3] S. V. Sattiraju, B. Dang, R. W. Johnson, Y. Li, J. S. Smith, M. J. Bozack, *IEEE T. Electron. Pack.* 2002, *25*, 1338.
[4] Yeonjin Yi, Sangwan Cho, Myungkeun Noh, Chung-Nam Whang, Kwangho Jeong, Hyun-Joon Shin, *Jpn. J. Appl. Phys.* **2005**, *44*, 861.
[5] H. P. Zeindl, S. Nilsson, U. Jagdhold, J. Klatt, R. Kurps, D. Kruger, E. Bugiel, *Appl. Surf. Sci.* **1996**, *102*, 107.
[6] K. S. Kim, S. H. Huh, K. Suganuma, *J. Alloy. Compd.* **2003**, *352*, 226.
[7] C.-Ming Chuang, P.-C. Shi, K.-L. Lin, *Int'l Symposium on Electronic Materials and Packaging(IEEE)* **2002**, *2002*, 360.
[8] R. J. Coyle, P. P. Solan, A. J. Serafino, S. A. Gahr, *Electron. Components and Technol. Conf.(IEEE)* **2000**, *50*, 160.
[9] C. H. Zhong, S. Yi, *Solder. Surf. MT. Techn.* **1999**, *11*, 44.

DOI: 10.1002/adem.200500164

Correlating Interfacial Moisture Content and Adhesive Fracture Energy of Polymer Coatings on Different Surfaces

By *Emmett P. O'Brien, Christopher C. White,* Bryan D. Vogt**

It is well known that ambient moisture and other environmental influences are detrimental to the adhesion of polymeric materials to metal surfaces. The primary reason why adhesion loss occurs is believed to be due to moisture accumulation at the polymer/metal interface. This is why adhesion loss does not generally correlate with the bulk moisture content of the polymer. In this work, we present measurements of the interfacial moisture content and adhesion for a series of polymer coatings having different surface chemistries. Measurements were made after reaching an apparent equilibrium in either a dry (0 % relative humidity) or wet (100 % relative humidity) environment. The loss of adhesion is found to correlate directly with interfacial water content. Surface treatments that resulted in a more hydrophilic surface lead to an increase in the interfacial water content and a decrease in interfacial fracture energy.

Ambient moisture is well known to adversely affect the durability and performance of adhesive joints and coatings.[1] The interplay between the mechanical stress and chemical changes in the adhesive joint due to moisture adsorption is generally believed to be the root cause of failure of the adhesive application. Failure typically occurs at the polymer/metal interface, indicating that the primary mechanism for failure is not degradation of the bulk polymer. Instead, the structure of the coating near the interface is the determining factor in

[*] *Dr. E. P. O'Brien, Dr. C. C. White*
National Institute of Standards and Technology
Buildings and Fire Research Laboratory
Gaithersburg, MD 20898
E-mail: cwhite@nist.gov
Dr. B. D. Vogt
National Institute of Standards and Technology
Polymers Division
Gaithersburg, MD 20898
E-mail: bryan.vogt@nist.gov
Dr. E. P. O'Brien
Eastman Chemical Company
P.O.Box 1972
Kingsport, TN 37662, USA

ADVANCED ENGINEERING MATERIALS

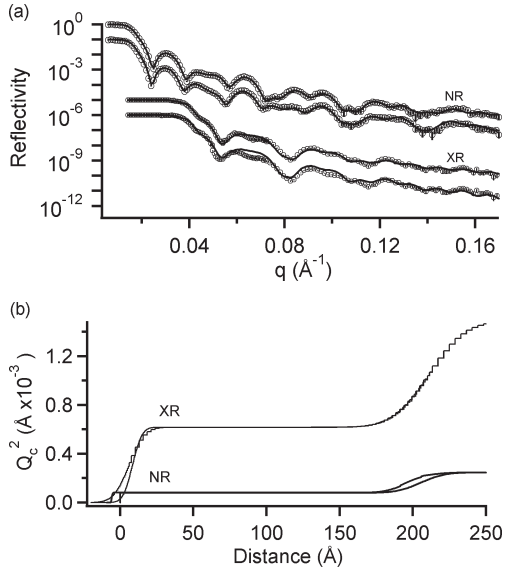

Fig. 1. (a) Neutron (top set) and x-ray reflectivity (bottom set) profiles of PBOCSt film on alumina before (upper curve) and after (lower curve) exposure to saturated D_2O vapor. The solid lines correspond to fits of the data. Data are offset for clarity. (b) Scattering length density profiles obtained from fits of the reflectivity profiles.

the adhesive failure in most coatings, so understanding the interface is critical to predicting adhesive joint durability. Past work has shown evidence for a moisture rich environment near the interface[2–5] and has identified the interface as an important pathway for moisture transport;[3,6–8] however, quantification of the distribution has remained elusive. Recently, the high spatial resolution of neutron reflectivity (NR) has allowed for the quantification of the gradient of moisture content away from the buried polymer/metal interface.[9–14] Two general conclusions may be drawn from previous research examining the moisture distribution in adhered polymer films. First, the moisture content at the polymer/substrate interface is largely independent of the polymer.[10,13] Second, the moisture content is strongly dependent upon the underlying substrate surface chemistry.[14] To date, this moisture content has not been directly related to the adhesive performance of these materials. Kramer and co-workers have used NR to examine the local crosslink density of epoxy resins near surfaces and have correlated this crosslink density with the fracture energy of these joints.[15] However, this study was limited to dry samples. In many applications, adhesive joints are exposed to harsh environments that lead to a significant decrease in the adhesive fracture resistance. In this work, we have attempted to correlate adhesive fracture energy (or strain energy release rate) of polymer films with moisture content at the buried interface. NR has been used to quantify the moisture content at the polymer/substrate interface for a series of substrate surfaces. The shaft-loaded blister test (SLBT) has been utilized to measure adhesion[16–24] and mechanical properties of the adhered thin films.[16,20,25–30] Using neutron reflectivity and SLBT adhesion measurements, we investigate how surface chemistry influences the water content near the interface and the adhesive fracture energy after attaining an apparent equilibrium in either the dry (0 % relative humidity (rh.) and wet (100 % rh.) state.

Reflectivity measurements of film structure: Figure 1(a,b) shows the neutron and X-ray reflectivity profiles for samples measured under vacuum (dry) and exposed to saturated D_2O vapor at ambient temperature (wet). Figure 1(a) shows the reflectivity measured as a function of the momentum transfer vector, q, where $q = 4\,\delta/\lambda\,\sin(\theta)$, where λ is the wavelength and θ is the incident angle. Figure 1(b) shows the scattering length density profile, where the distance on the x-axis is measured from the air/coating interface (0 Å) obtained in the dry condition. The scattering length density profiles in Figure 1(b) correspond to the fit of the data shown by the solid line in Figure 1(a). The goodness of the fit is representative of all datasets. As shown in Figure 1(b), upon exposure to D_2O vapor, NR changes are detected at the alumina/polymer, shown between a distance of 175 and 250 Å. However, Figure 1(b) also shows that changes near the interface are not detected with X-ray reflectivity (XR). This apparent contradiction is due to the difference in the source of contrast for XR and NR, and therefore the sensitivity of each technique. XR is sensitive to the sample electron density, which closely follows the physical density, whereas NR is sensitive to the neutron scattering length density (NSLD). For these experiments, the electron density of D_2O is similar to the polymer coating, whereas the NSLD of D_2O is more similar to the alumina. As a consequence of the similarity between the electron density of D_2O and the polymer, XR measures solely changes in thickness. However, changes in D_2O concentration near the polymer/substrate interface can be detected due to the difference in NSLD between the polymer, D_2O and substrate. Using a procedure described previously by Vogt et. al., the NSLD profiles were converted into water concentration profile away from the interface.[13,14] Figure 2 shows the water concentration profiles for the different surfaces: bare alumina (Al_2O_3), native silicon oxide (SiO_x), phenylphosphonic acid treated alumina (phenyl), t-butylphosphonic acid treated alumina (t-butyl), and n-octyltrichlorosilane (OTS) treated alumina (octyl). For a direct comparison of the alumina and silicon oxide surfaces, the water profiles are shown as the distance from the center of the dry oxide/polymer interface. As the surface becomes more hydrophobic, the water concentration near the interface decreases. This is tabulated in Table 1;

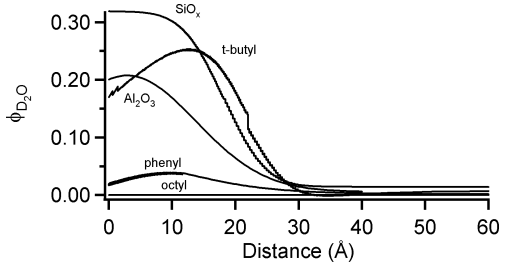

Fig. 2. Water concentration profiles obtained for PBOCSt films on different surfaces. The distance is polymer/substrate interface midpoint in order to facilitate direct comparison of the SiO_x (sharp interface) and different alumina surfaces (diffuse interface).

Table 1. The contact angle of water (°) and maximum interfacial moisture content (%) as function of the adherend surface chemistry. Surfaces are shown in order of increasing hydrophobicity.

	SiO_x	Al_2O_3	t-butyl.	phenyl.	octyl.
Contact Angle (°)	0°	60°	74°	78°	95°
Moisture Concentration (%)	32	21	25	4	<1

illustrating the contact angle of water and the maximum water concentration near the interface as a function of the adherend surface chemistry. The silicon oxide surface is the most hydrophilic surface (lowest water contact angle) and has the largest interfacial moisture concentration. Conversely, the OTS treated surface is the most hydrophobic surface and exhibits the lowest interfacial moisture content.

Adhesion measurements on different surfaces: Identical surfaces were prepared for SLBT specimens to correlate the moisture content as determined by NR measurements to the adhesive fracture energy, G, of the interface. The blister height, w, as a function of blister radius, a, for the different surfaces and before and after moisture exposure are shown in Figure 3(a). Two different failure mechanisms were observed. The dry specimens except the OTS-coated surface exhibit cohesive slip-stick failure. In contrast to the dry specimens, the wet specimens (exposed to saturated vapor) failed interfacially except for the phenylphosphonic acid treated surface. Future work using XPS and AFM will be carried out to quantify the failed fractured surface. The change in the failure mechanism between wet and dry samples is likely a result of the interfacial moisture accumulation. For these surfaces, significant accumulation is observed as previously illustrated in Figure 2. Much less moisture is found at the polymer/phenyl interface and thus this specimen fails cohesively in both the dry and wet states. The low surface energy of the OTS leads to inherently poor interfacial strength and subsequently interfacial failure is observed for both the dry and wet states. This work shows that surface chemistry and interfacial water content are important factors in determining the adhesive failure mechanism.

The energy release rates for dry and wet specimens as a function of the adherend surface chemistry are shown in Figure 3(b). This work also shows that the adhesive fracture energy of the exposed adhesive joints and coatings depend largely on the amount of moisture at the buried interface. As expected, the contact angle of water correlates well to the dry adhesion. Low water contact angle surfaces correspond to large dry adhesion. The large standard deviation is an artifact of the exponent in Equation 1 (see experimental section) used to calculate G. Therefore, small differences in w and a result in large changes in the calculated value of G. The adhesion between PMMA and SiO_x in the dry state is so large that in one case the film ruptured during fracture testing. The Al_2O_3 also exhibits large value of G in dry conditions, comparable to the SiO_x surface. For both surfaces, the strong adhesion is probably attributable to the oxidized surface which can form secondary bonds with the adhesive. However, roughness of the Al_2O_3 surface may also impart other beneficial effects.[1] The treated surfaces with hydrocarbon moieties all exhibit substantially lower adhesion in comparison to the oxides. This decrease is suspected to be due to the large dispersive component of the total surface energy and the blocking of the favourable oxide sites on the underlying substrate.

Correlation between interfacial moisture content and adhesion loss: The adhesive fracture energy dramatically changed after exposure to moisture. The most dramatic change in fracture energy occurred for the SiO_x substrate. The same silicon oxide moieties that result in large dry adhesion also readily attracts moisture, leading to the most water rich interface (32 %) and worst wet adhesion ($G = 0.02 \pm 0.03$ J/m^2). After moisture exposure, the Al_2O_3 and t-butyl samples have similar energy release rates, although the interfacial water concentration is slightly larger for t-butyl (25 %) than Al_2O_3 (21 %). The large moisture content for the t-butyl surface is uncharacteristic of hydrocarbon surface treatments, which generally reduces moisture accumulation near the interface. This issue with the t-butyl surface will be addressed later. The phenyl treated surface has the best wet adhesion of surfaces tested and exhibited relatively low interfacial moisture content (4 %). The octyl surface shows essentially no interfacial moisture content after exposure (< 1 % interfacial moisture content). As a consequence, there is no change in the adhesion between the dry and wet states for the octyl surface. The interfacial water content and the adhesive fracture energy appear corre-

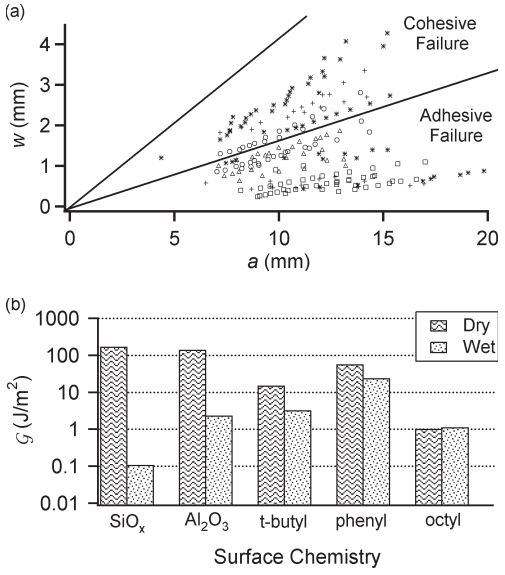

Fig. 3. (a) Scatter plot of the shaft-loaded blister test results. The displacement (blister height), w, is shown as a function of the blister radius, a for SiO_x (+), Al_2O_3 (*), t-butyl. (Δ), phenyl (○), and OTS (□) surfaces. The plot is split up into samples that showed cohesive failure and that which showed adhesive failure. (b) The energy release rate (G) as a function of surface chemistry for wet and dry adhesion.

ADVANCED ENGINEERING MATERIALS

lated, where increasing the interfacial water content tends to decrease the adhesive fraction energy.

The accumulation of moisture at the buried interface is a destabilizing force in the adhesion of the polymer to the substrate. In Figure 4(a), the loss of adhesion with moisture content is illustrated. In general, there is a trend where increasing moisture content leads to greater adhesion loss. However, this trend does not hold for the t-butyl surface. This was unexpected given that the hydrophobic pendent methyl groups should cover the surface. The t-butyl surface examined exhibits interfacial moisture content similar to untreated Al_2O_3. The water contact angle (74°) is significantly lower than would be expected for a fully methylated surface (90°) suggesting that partial surface coverage of *t*-butyl is responsible for the poor wet adhesion. The areas of the surface covered by the *t*-butyl tend to decrease the dry adhesion and breaks in surface coverage allow water to accumulate at the interface and coordinate with the phosphonic acid moiety,[14] leading to destabilization of the interface under load.

The relative loss of adhesion upon moisture exposure is not the important factor from an application standpoint, but rather the fracture energy after exposure in a moist environment. Surface modifications that prevent moisture accumulation also decrease dry adhesion. As an example, although there is no adhesion loss by moisture exposure for the octyl surface, the adhesive strength in both the wet and dry states is lacking. The adhesion strength in the wet state for the different surfaces is shown in Figure 4(b) as a function of interfacial moisture content. *G* decreases with increasing interfacial moisture content except for the case of the octyl surface. This illustrates the interplay between hydrophobicity of the substrate leading to poor adhesion and interfacial water leading to adhesion loss. For the phenyl surface, the failure mechanism is cohesive, not interfacial as the case for all other surfaces in the wet state. It appears that the interfacial water content for the phenyl surface is insufficient to cause significant degradation of the interface and the surface is not so overly hydrophobic that the adhesion in general is poor. Not coincidentally this surface exhibits the best wet adhesion.

Summary: The adhesion of polymer film of PMMA to different surfaces was measured using the shaft-loaded blister test. The exposure of the films to saturated water vapor generally leads to a decrease in adhesive strength. The adhesion loss was directly related to the moisture accumulation at the polymer/substrate interface as measured using neutron reflectivity. In a dry environment, high surface energy substrates lead to greater dry adhesion, but larger adhesion loss during exposure to moisture and accompanying larger interfacial water content. There is interplay between interfacial moisture content and surface hydrophobicity in the case of wet adhesion. One surface treated with OTS exhibited no adhesion loss upon exposure to moisture as no water accumulated at the interface, but the dry adhesion was poor rendering this treatment unfavorable for applications. The best wet adhesion was found for a phenyl phosphonic acid treated surface where the surface treatment limited the moisture accumulation at the buried interface while not completely degrading the adhesion in the dry state. As a guideline for polymer adhesion to surfaces in moist environments, complete surface coverage by a moderately hydrophobic moiety should lead to the best performance based upon the interplay between dry adhesion and interfacial moisture accumulation.

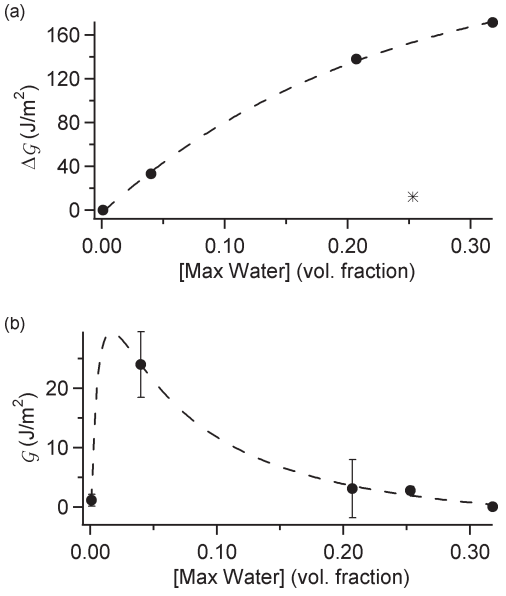

Fig. 4. Correlation of energy release rate with the moisture accumulation at the buried interface. (a) The change in the average energy release rate between the dry and wet states for the same surface is shown as a function of interfacial moisture content. The t-butyl surface (*) does not follow the trend presumably due to incomplete surface coverage (b) The energy release rate in the wet state decreases as the interfacial moisture content increases. The dashed lines are provided as a guide to the reader.

Experimental

Due to differences in the test geometry between the SLBT and NR, nominally identical independent samples were prepared for each experiment. Shaft-loaded blister test specimens (SLBT) were prepared on 0.32 mm thick Borofloat glass substrates with an 8 mm diameter hole bored through the center of the surface. The surfaces of some substrates were modified by evaporation of 40 nm of aluminum, which was subsequently oxidized in a ultraviolet (UV) ozone cleaner for 3 min. Further surface modification was possible by the use of organic phosphonic acids and n-octyltrichlorosilane (OTS). For this study, two different phophonic acids were examined: phenylphosphonic acid and t-butylphosphonic acid. Details of the surface treatment are provided elsewhere.[14] These different treatments resulted in 5 surfaces to examine.

A SLBT specimen must have a pre-crack to initiate debonding and the thin adhered film must be sufficiently mechanically reinforced such that the film will not rupture during application of the load. A pre-crack was created by placing a 0.95 cm diameter piece of Kapton pressure sensitive adhesive tape (PSAT) over the hole in the center of the Borofloat substrate. A nominally 15 μm thick film of poly(methyl methacrylate) (PMMA) was spin cast from 15 % by mass solution of PMMA in toluene. On top of the PMMA film, 1.1 mL of degassed Bisphenol-A resin cured with 43 phr Jeffamine T-403 curing agent was coated on the substrate. A 50 μm (2 mil) thick piece of Kapton-E film (no PSA) was then placed on top of the uncured epoxy resin for mechanical reinforcement. The entire composite film of PMMA/Kapton-E/epoxy film was allowed to cure at room temperature for 48 h, to reduce residual stresses that arise from the mismatch in the coefficient of thermal expansion between the adhesive and substrate, and then cured at 60 °C for 1 h. The thickness of the entire adhesive coating was nominally 100 μm. The modulus of the composite coating, σ_c, was estimated from the rule of mixtures, $\sigma_c = \sum \nu_i \sigma_i$, where σ_i and ν_i are the modulus and volume fraction of the *i*th component, respectively.

Specimens were conditioned at room temperature either in a dessicator (< 5% r.h.) or at 100%r.h.. Samples were tested after conditioning for three days, well beyond the time required to reach quasi-equilibrium assuming Fickian diffusion. Three or four samples were tested for each surface and moisture level using a universal testing machine (UTM) and shaft attached with a ball bearing approximately 0.63 cm in diameter. The maximum displacement during each cycle was either 0.5 or 1 mm and the UTM cross-head displacement rate was 0.1 mm/sec. The energy release rate was calculated from the displacement based equation:[20]

$$G = \frac{Eh}{16}\left(\frac{w}{a}\right)^4 \quad (1)$$

where w is the blister height or displacement, a is the debond radius, G is the modulus of the adhesive film and h is the adhesive thickness. Previous work suggested that the load-based equation is the preferred expression to calculate G due to the reduced effects of plastic deformation at the contact area and the insensitivity to changes in mechanical properties of the film[16,24] due to plasticization by fluid absorption.[23] However, in the presence of the slip-stick failure as observed for these samples, the displacement-based is the most appropriate expression to calculate G. Specimens were tested using loading and unloading cycles, which were repeated multiple times, to determine the crack length as a function of load and displacement (blister height). The uncertainty due to sample-to-sample variation is always equal to or greater than the uncertainty introduced by measuring the blister radius. For discussion, we refer in the text to "dry" and "wet" adhesion as the measured interfacial toughness, as determined by the energy release rate, for specimens conditioned in a dry environment and a 100% relative humidity, respectively.

Samples for NR and XR were prepared on silicon wafers. The alumina surface was prepared by directly sputtering alumina (40 nm) onto silicon wafer. The wafer contact angle of this alumina surface and the UV-ozone exposed evaporated aluminum was indistinguishable. Identical procedures to those previously described for the SLBT samples were used to prepare the surfaces. Previous studies have indicated that water accumulation at the buried interface is independent of polymer coating.[9–13] For consistency with previous studies, poly(t-butoxycarboxystyrene) was utilized as the polymer coating.[13,14] Neutron reflectivity experiments were performed on the NG7 reflectometer at the NIST Center for Neutron Research utilizing cold neutrons with a wavelength (λ) = 4.768 Å and wavelength spread ($\Delta\lambda/\lambda$) = 0.2. Data were collected at the specular condition. NR is capable of probing the neutron scattering density at depths of up to several thousand Å, with an effective depth resolution of ± 3 Å. To quantify the moisture distribution in the film, perdeuterated water (D_2O) was used for neutron contrast. The samples were measured initially under vacuum (dry) and then after exposure to saturated D_2O vapor at ambient temperature. XR measurements were conducted in a θ-θ configuration using Ni filtered CuK_α radiation (λ = 1.54 Å) and Soller slit collimation on the incident and reflected beams.

Received: July 20, 2005
Final version: September 02, 2005

[1] A. J. Kinloch, *Adhesion and Adhesives: Sci. and Technol.* Chapman and Hall: New York, **1987**.
[2] K. M. Takahashi, T. M. Sullivan, *J. Appl. Phys.* **1989**, *66*, 3192.
[3] T. Nguyen, E. Byrd, D. Bentz, *J. Adhesion* **1995**, *48*, 169.
[4] S. H. McKnight, J. W. J. Gillespie, *J. Appl. Polym. Sci.* **1997**, *64*, 1971.
[5] S. Affrossman, W. M. Banks, D. Hayward, R. A. Pethrick, *Proc. Inst. Mech. Eng.* **2000**, *214*, 87.
[6] M. P. Zanni-Deffarges, M. E. R. Shanahan, *Int. J. Adhes. Adhes.* **1995**, *15*, 137.
[7] E. P. O'Brien, P. F. Reboa, M. Field, D. Pullen, D. Markel, T. C. Ward, *Int. J. Adhes. Adhes.* **2003**, *23*, 335.
[8] G. D. Davis, L. A. Krebs, L. T. Drzal, M. J. Rich, P. Askeland, *J. Adhesion* **2000**, *72*, 335.
[9] W. L. Wu, W. J. Orts, C. J. Majkrzak, D. L. Hunston, *Polym. Eng. Sci.* **1995**, *35*, 1000.
[10] M. S. Kent, G. S. Smith, S. M. Baker, A. Nyitray, J. Browning, G. Moore, D. Hua, *J. Mater. Sci.* **1996**, *31*, 927.
[11] M. S. Kent, W. F. McNamara, D. B. Fein, L. A. Domier, A. P. Y. Wong, *J. Adhesion* **1999**, *69*, 121.
[12] M. S. Kent, W. F. McNamara, P. M. Baca, W. Wright, L. A. Domier, A. P. Y. Wong, W. L. Wu, *J. Adhesion* **1999**, *69*, 139.
[13] B. D. Vogt, C. L. Soles, R. L. Jones, C. Y. Wang, E. K. Lin, W. L. Wu, S. K. Satija, D. L. Goldfarb, M. Angelopoulos, *Langmuir* **2004**, *20*, 5285.
[14] B. D. Vogt, V. M. Prabhu, C. L. Soles, S. K. Satija, E. K. Lin, W. L. Wu, *Langmuir* **2005**, *21*, 2460.
[15] J. J. Benkoski, E. J. Kramer, H. Yim, M. S. Kent, J. Hall, *Langmuir* **2004**, *20*, 3246.
[16] E. P. O'Brien, T. C. Ward, S. Guo, D. A. Dillard, *J. Adhesion* **2003**, *79*, 69.
[17] K. Liao, K. T. Wan, *J. Mater. Sci. Lett.* **2000**, *19*, 57.
[18] K. Liao, K. T. Wan, *J. Compos. Techn. Res.* **2001**, *23*, 15.
[19] K. T. Wan, A. DiPrima, L. Ye, Y. W. Mai, *J. Mater. Sci.* **1996**, *31*, 2109.
[20] K. T. Wan, Y. W. Mai, *Int. J. Fract. Mech.* **1995**, *74*, 181.
[21] K. T. Wan, Y. W. Mai, *Mater. Sci. Res. Int.* **1995**, *1*, 78.
[22] X. J. Xu, C. Shearwood, K. Liao, *Thin Solid Films* **2003**, *424*, 115.
[23] E. P. O'Brien, S. L. Case, T. C. Ward, *J. Adhesion* **2005**, *81*, 41.
[24] E. P. O'Brien, S. Goldfarb, C. C. White, *J. Adhesion* **2005**, *81*, 599.
[25] K. T. Wan, K. Liao, *Thin Solid Films* **1999**, *352*, 167.
[26] K. T. Wan, *J. Adhesion* **1999**, *70*, 209.
[27] K. T. Wan, S. Guo, D. A. Dillard, *Thin Solid Films* **2003**, *425*, 150.
[28] B. F. Ju, K. K. Liu, S. F. Ling, W. H. Ng, *Mech. Mater.* **2002**, *34*, 749.
[29] M. R. Begley, T. J. Mackin, *J. Mech. Phys. Solids* **2004**, *52*, 2005.
[30] U. Komaragiri, M. R. Begley, J. G. Simmonds, *J. Appl. Mech.* **2005**, *72*, 203.

